Available online at www.sciencedirect.com
ScienceDirect
Cement and Concrete Research 38 (2008) 467–476
Cement and Concrete Research

Surface roughness criteria for cement paste nanoindentation

Mahalia Miller, Christopher Bobko, Matthieu Vandamme, Franz-Josef Ulm *

Massachusetts Institute of Technology, Cambridge MA, United States

Received 5 September 2007; accepted 29 November 2007

Abstract

Analysis of nanoindentation experiments assumes that the indentation occurs on a flat surface. As a result, the accuracy of nanoindentation depends on reducing the surface roughness to a tolerable level. Within the context of statistical nanoindentation techniques suitable for heterogeneous materials, this study presents a criterion for roughness of cement paste surfaces for nanoindentation, and describes a method for obtaining the desired roughness. Through a systematic experimental study, we show the evolution of roughness and nanomechanical properties from indentation as a function of increased polishing. We conclude that the root-mean-squared (RMS) roughness of the sample, taken over a square area with edge dimensions of 200 times the average indentation depth of the dominating phase of the material, should be less than five times the average indentation depth of the dominating phase of the material.

Keywords: Nanoindentation; Atomic Force Microscopy; Roughness; Cement paste; Sample preparation

1. Introduction

The grid nanoindentation technique has been proven to provide useful, quantitative information about the mechanical behavior of cement pastes at the nanoscale [1–5]. The technique extends nanoindentation tools that had previously been limited to homogeneous materials and thin films to complex heterogeneous composites. Its attractiveness stems largely from the fact that properties of mechanically meaningful material phases can be identified in situ by performing large grids of indentations on highly heterogeneous samples, with a proper choice of the indentation depth to ensure the self-similar properties of classical continuum indentation analysis [6]. One challenge in the application of nanoindentation to cement pastes, however, is the development of a surface preparation technique that minimizes both sample disturbance and surface roughness. A further challenge is understanding how rough a surface can be without affecting the results of nanoindentation.

Analysis of individual indentation tests using the conventionally applied Oliver and Pharr method [7] assumes that the initial surface is perfectly flat. Classical tools of indentation analysis, based on the infinite half-space model, can then be applied. Given this assumption, indentation with a Berkovich indenter can be considered to be self-similar. Since the infinite half-space model has by definition no length scale, dimensional analysis reveals that, for a homogeneous material, results of an indentation test do not depend on any other length scale than the indentation depth [8,9]. It is then readily understood that the presence of significant surface roughness introduces a new length scale into the dimensional analysis, which breaks the self-similarity of the indentation test and introduces a link between measured properties and indentation depth. Indeed, experimental evidence from prior research shows that the presence of significant surface roughness tends to increase the scatter in measured indentation modulus and indentation hardness, along with an overall reduction in these properties [10–12]. An ISO Standard dealing with nanoindentation warns that "surface finish has a significant influence on the test results" [15]. The question to be solved is, how small must the surface roughness be, in comparison with the indentation depth, to not have an effect on the measured mechanical properties?

Some researchers have approached a slightly different question and introduced corrections to the contact depth based on measurements of the roughness of the sample to be indented [10,11]. These procedures have two important limitations. First,

* Corresponding author. Tel.: +1 617 253 3544; fax: +1 617 253 6044.
E-mail address: ulm@mit.edu (F.-J. Ulm).

0008-8846/$ - see front matter © 2007 Elsevier Ltd. All rights reserved.
doi:10.1016/j.cemconres.2007.11.014

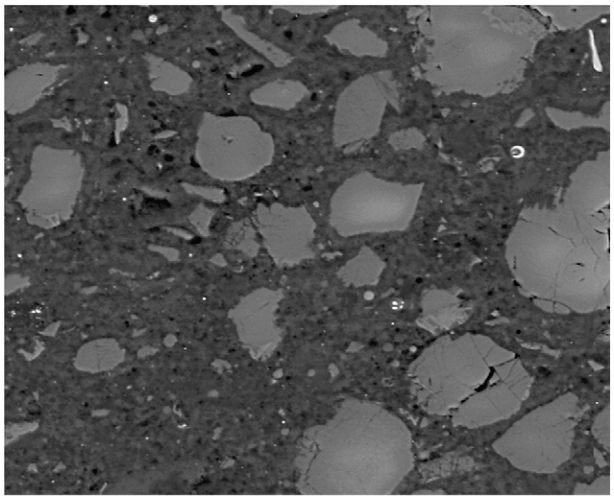

Fig. 1. Back-scattered electron image of the fully polished surface. The image is taken in a FEI/Philips XL30 FEG ESEM at 15 kV. The width of the image is 100 μm.

the quantification of surface roughness is not a standard procedure; different experimental parameters can yield different results. Second, the proposed corrections are most directly applicable for relatively small roughness compared to the overall indentation depth. Other researchers have sought to avoid the need for corrections by giving a criterion on the average, R_a, or root-mean-squared (RMS), R_q, roughness, as a function of maximum indentation depth. This criterion identifies a surface roughness that closely approximates the assumption of indentation on a perfectly flat surface. The ISO Standard references a study investigating the effect of roughness on hardness measurements of metals [16] which gives a criterion of $h_{max} > 20R_a$. For Berkovich indentation on cancellous bone, a preliminary criterion of $h_{max} > 3R_q$ has been given by Donnely et al. [12]. Donnely's criteria are also limited by the lack of a standardized method for determining the RMS roughness.

Atomic Force Microscopy (AFM) is an increasingly popular tool for researchers studying cement-based materials. Researchers have studied surface topography to understand cement hydration [17], response to relative humidity [18], and the effect of pozzolanic additives on microstructure [19]. Others have extended the experimental technique to study the attractive forces at the origin of cement cohesion [20,21] and to use the AFM probe as an indenter to assess mechanical properties [22]. In this study, AFM is employed in a more conventional manner to provide a good assessment of the surface topography of a cement sample.

This paper presents a polishing procedure that minimizes the surface roughness of a cement paste, and presents a criterion for roughness of cement pastes for nanoindentation. Atomic Force Microscopy is used to visualize and quantify the roughness of a sample at varying states of polishing. An experimental nanoindentation campaign on the same sample with a series of decreasing roughnesses demonstrates the effect of surface roughness on statistical indentation results. Using the nanoindentation results from the fully polished sample as control variables, the evolution of nanoindentation results with surface roughness obtained from AFM imaging gives the basis for a new criterion for surface roughness of cement pastes to be tested by nanoindentation. This new criterion includes consideration of the multi-phase composite nature of the cement paste and consideration of the method for determining surface roughness.

2. Materials and methods

2.1. Materials

This paper presents a case study of a cement paste prepared at a water-to-cement ratio of $w/c = 0.2$ using alite-rich cement from Le Teil. The chemical composition of the cement (by mass) is 69.5% alite, 17% belite, 4.5% ferrite, and 2.4% aluminate. The Blaine fineness of the cement, obtained from laser granulometry, is 2940 cm^2/g. The sample contains 24% silica fume (by mass), with Blaine fineness, obtained from laser granulometry, of 2550 cm^2/g. After 2 days of hydration, the sample was subjected to a heat treatment of 90 °C for 2 days. The rationale for choosing such a low w/c ratio material for this study is that the hardened material is expected to contain, in addition to calcium-silicate hydrates (C–S–H), a relatively large amount of unhydrated clinker; thus leading to the highest possible contrast in mechanical properties between indented material phases. Fig. 1 shows the expected high concentration of unhydrated clinker.

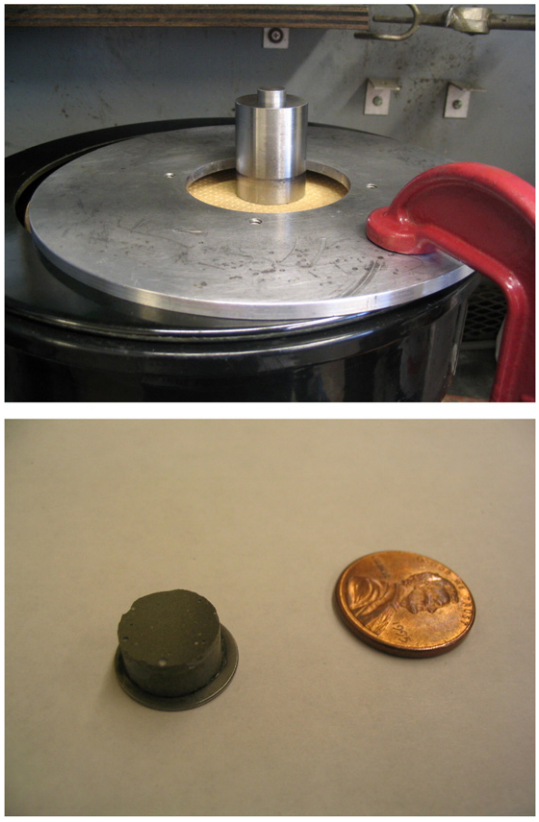

Fig. 2. Top: Equipment used to polish specimen. The sample rests face down on the TexMet P pad, inside the stainless steel jig. The inner cylinder, which is free to move up and down, rests on the back of the stainless steel mounting plate. The metal collar holds the jig in place on the lapping wheel and pad while allowing the jig and sample to rotate freely. Bottom: Sample on a mounting plate.

2.2. Surface preparation

There are three primary goals of the surface preparation procedure: (1) to achieve as flat a surface as possible, (2) to obtain repeatable results, and (3) to minimize the sample disturbance. The procedure described here is optimized to satisfy these three goals:

1. The first step is to trim the sample to an appropriate size using a diamond saw. Specimens were cut into 3–8 mm thick disks of 10 mm, and then mounted on a stainless steel AFM specimen disk (Ted Pella) using a thin layer of cyanoacrylate as an adhesive.
2. The second step is a coarse grinding step. The goal of this step is to make the top of the sample parallel with the bottom of the specimen disk, so there is no tilt to the surface during indentation. The sample is placed in the specially designed jig consisting of a stainless steel outer sleeve, with an opening drilled through to match the diameter of the specimen disk. An interior cylinder fits closely inside, and rests on the back of the specimen disk to apply a light weight to the sample (see Fig. 2). Inside the jig, the sample is ground on 120 grit ZirMet (Buehler) abrasive paper. The amount of material removed is not measured, but grinding proceeds until the entire surface has been ground. Keeping the sample relatively short and wide compared to the specimen disk helps to prevent the sample from tilting and creating a convex surface. The sample and the jig are then cleaned separately, with the sample in *n*-decane and the jig in water, in an ultrasonic bath for 5 min. An AFM topographic image of the results of this step is shown in Fig. 3(a).
3. The third and final step is the polishing step. After much trial and error with a variety of polishing compounds and polishing mats, one combination gave us repeated success. A TexMet P (Buehler) pad, a hard, perforated, non-woven pad is mounted to a lapping wheel. The hardness of the pad assures that the highest surfaces of the sample are removed first, and the perforation gives a place for the polishing residue to collect without interfering with the polishing itself. This is particularly important because the described polishing process does not

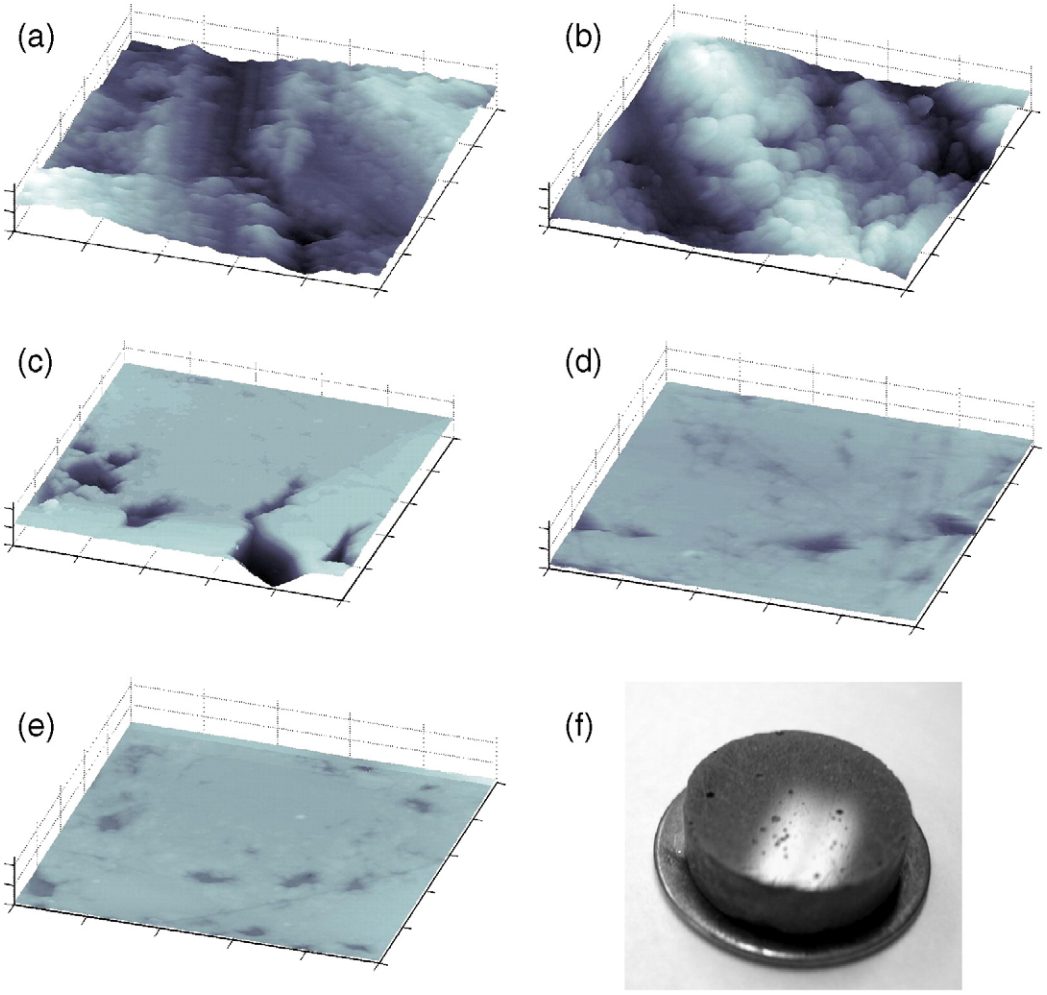

Fig. 3. AFM images of different stages of the polishing process and a photograph of the sample showing the final polished surface. Each AFM image is of a 50 μm by 50 μm area, and the maximum value of the height axis for each image is 5000 nm. Image (a) is of the rough ground sample surface. Image (b) is taken after 1 h of polishing and minor flattening of the surface is visible. Image (c) is taken after 2 h. At this stage, the highest surfaces are flat and polished, but lower surfaces are still rough. Image (d) is taken after 4 h. As polishing continues, the surface is nearly flat across the entire area. Image (e) is taken after the full 8 h of polishing. Image (f) is a photograph showing the reflective sample surface after the full 8 h of polishing.

include any ongoing cleaning of the pad. The TexMet P pad is charged with approximately 0.5 mL of 1 μm oil-based diamond suspension (Metadi, Buehler). A polishing fluid helps to dissipate any heat build-up, and the oil-base specifically helps to prevent any further hydration and change in water-to-cement ratio. Using only one size of diamond suspension aids in the repeatability of the procedure, as there is no need for the extensive cleaning required if the sample were polished by a series of smaller and smaller diamond suspensions. While this may result in a longer polishing time, it requires much less operator intervention, and therefore increases the repeatability of the procedure. The sample and jig are held on the pad, approximately 3 to 4 cm from the center of the lapping wheel, and the jig is allowed to freely rotate. The wheel is then spun at 1 cps, so a typical velocity underneath the sample is 18 to 25 cm/s. The relatively slow lapping speed is essential in minimizing the sample disturbance and creating a smooth surface. This polishing lasts for 8 h. As before, the sample and the jig are then cleaned separately, with the sample in *n*-decane and the jig in water, in an ultrasonic bath for 5 min.

Fig. 3(b)–(d) shows the progression of the surface after 1 h, 2 h, and 4 h of total polishing time. After 1 h of polishing, the surface is a bit smoother overall, but dramatic change is seen after 2 h. Here, the high surfaces have been polished flat, while lower surfaces are still rough. The remaining polishing removes all the higher material to create a uniformly flat surface. The final results of this polishing are shown in Fig. 3(e). After the full 8 h of polishing, inspection of the clean surface by the naked eye reveals a mirror-like finish that reflects overhead light, as shown in Fig. 3(f). The overall material removed was not measured, but from a careful analysis of the AFM images, the material removal rate is at least on the order of 1 μm per unit area per hour.

2.3. Statistical nanoindentation technique

Nanoindentation consists of making contact between a sample and an indenter tip of known geometry and mechanical properties, followed by a continuously applied and recorded change in load, P, and depth, h. Typical tests consist of a constantly increasing load, followed by a short hold and then a constant unloading; a P–h curve is reported. The analysis of the P–h curve proceeds by applying a continuum scale model to derive an indentation modulus, M, and hardness, H:

$$M = \frac{\sqrt{\pi}}{2}\frac{S}{\sqrt{A_c}} \tag{1}$$

$$H = \frac{P}{A_c} \tag{2}$$

where $S = \frac{dP}{dh}|_{h=h_{max}}$ is the (measured) initial slope of the unloading branch of the P–h curve, P is the (measured) maximum indentation load, and A_c is the projected contact area of the indenter on the sample surface. Using the Oliver and Pharr method, the projected contact area, A_c, is determined as a function of the (measured) maximum indentation depth, h_{max} [7]. The samples were tested with a CSM indenter at MIT, Cambridge, MA, using a diamond Berkovich tip.

2.3.1. Nanoindentation on cement pastes and deconvolution technique

Recognizing the high heterogeneity of cement paste at the nano- and micro-scale, applying the indentation technique is a challenge, as it is difficult to choose to indent on a specific material phase with sufficient repeatability. To address this challenge, it is advantageous to perform large grids of indentations on heterogeneous samples, such as cement paste [2,6,4,3]. Then, if the grid size and indentation depth are chosen properly, each indentation test may be treated as an independent statistical event; and a subsequent statistical deconvolution of the indentation results can be applied.

Briefly, we recall that the deconvolution technique consists of fitting the experimental cumulative distribution function (CDF) of the measured indentation modulus M and indentation hardness H, to the sum of model-phase CDFs [5]:

$$\min \sum_{i=1}^{N} \sum_{X=(M,H)} \left(\sum_{j=1}^{n} f_j D\left(X_i; \mu_j^X, s_j^X\right) - Dx(X_i) \right)^2 \quad \text{s.t} \quad \sum_{j=1}^{n} f_j = 1 \tag{3}$$

where D_X (X_i) are the experimental CDFs generated from N indentation tests performed on a specimen surface:

$$D_X(X_i) = \frac{i}{N} - \frac{1}{2N};\ \text{for } i \in [1;N];\ X = (M,H) \tag{4}$$

f_j stands for the surface fraction of each phase $j=1$, n occupies the indented surface; while $D(X_i;\ \mu_j^X,\ s_j^X)$ is the (assumed) Gaussian distribution of each phase, identified by the mean values μ_j^M and μ_j^H and the standard deviations s_j^M and s_j^H, of the indentation modulus M and the indentation hardness H, respectively:

$$j = 1, n; \tag{5}$$

$$D\left(X_i; \mu_j^X, s_j^X\right) = \frac{1}{s_j^X\sqrt{2\pi}} \int_{-\infty}^{X_i} \exp\left(\frac{-\left(u-\mu_j^X\right)^2}{2\left(s_j^X\right)^2} \right) du; X = (M,H).$$

Finally, to ensure that phases have sufficient contrast in properties, and thus to avoid the overlap of two neighboring Gaussians, the optimization problem is additionally constrained by:

$$\mu_j^X + s_j^X \le \mu_{j+1}^X - s_{j+1}^X,\ X = (M,H) \tag{6}$$

The results of the deconvolution technique are estimates of the $n \times 5$ unknowns $\{\mu_j^M,\ s_j^M,\ \mu_j^H,\ s_j^H,\ f_j\}$, $j=1,\ n$; that is, the

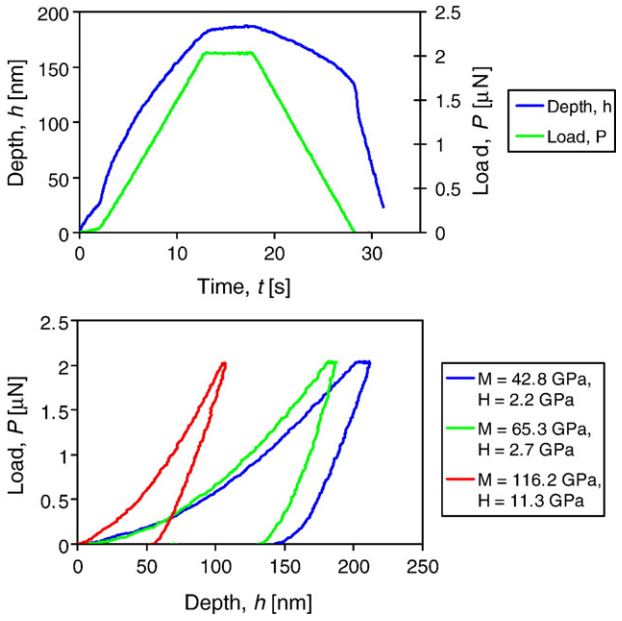

Fig. 4. Top: Indentation load vs. depth curves, with the derived indentation modulus and hardness. Each curve is characteristic of the response of a different material phase. Bottom: Indentation load vs. time and indentation depth vs. time for a typical indent.

mean and standard deviation of indentation modulus and hardness for each mechanical phase, and the surface fraction. For randomly organized materials, which is the case of cement paste [5], the surface fractions are actually volume fractions. Finally, it is worthwhile mentioning that the deconvolution technique here described differs from the original deconvolution technique suggested earlier [3,4] in that it is analytically more convenient to deconvolute the cumulative distribution function (CDF) rather than the probability density function (PDF), because generation of the experimental PDF requires a choice of bin-size for histogram construction.

Indentation testing employed in this study uses parameters that satisfy the assumptions of the grid indentation technique. For each series of indentation testing, 300 individual indentations were performed, on a grid of 20×15 with a spacing between indents of 20 μm. After making contact with the sample, the indenter applied a maximal load P_{max}=2 mN on the indenter tip and measured the displacement of the tip orthogonal to the surface of the sample. The load was increased linearly at 12 mN/min for 10 s, held at P_{max} for 5 s, and then unloaded in 10 s, following an established procedure [3]. This loading resulted in measured displacements which were typically between 100 and 400 nm. Fig. 4 (top) displays load vs. time and depth vs. time for one typical indentation experiment. As the bulk of the creep deformation in the holding step takes place in the first 1 to 2 s, 5 s is an adequate holding time for this material. Fig. 4 (bottom) displays three typical indentation responses, each corresponding to a different material phase.

By way of illustration, Fig. 5 shows the results of the deconvolution technique in terms of both CDFs and the PDFs for indentation modulus and indentation hardness for

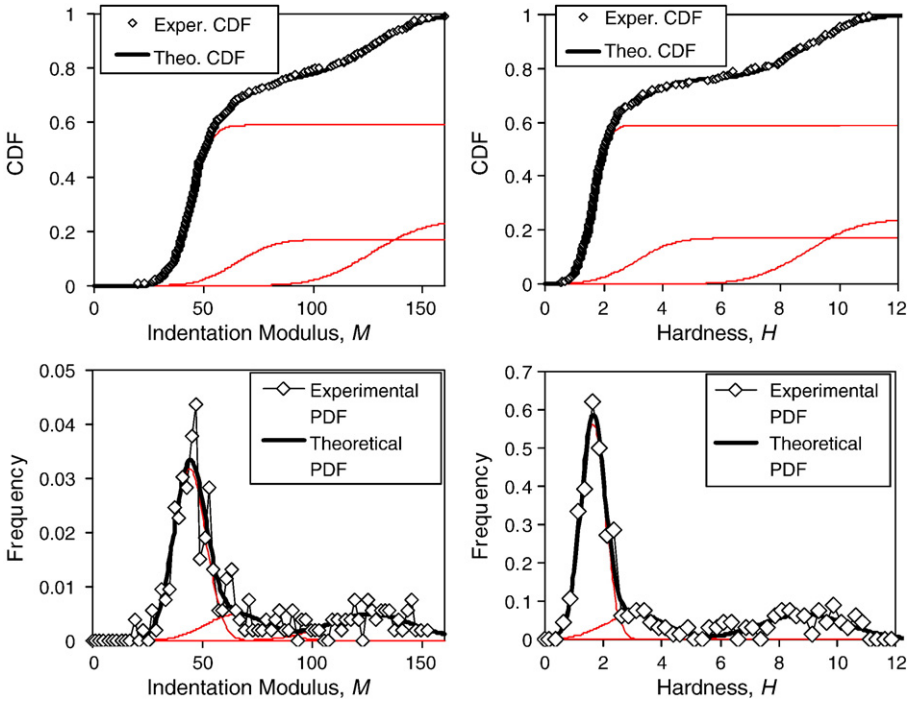

Fig. 5. Statistical indentation analysis of the cement paste: cumulative distribution functions (CDF — top) and probability density functions (PDF — bottom) of indentation modulus, M, (left) and hardness, H (right). The experimental CDF is constructed from the (M, H) data points from a 20 by 15 grid. It is deconvoluted in a series of three phase-specific CDFs, which are assumed to be Gaussian, and which are also displayed.

Table 1
Variability of the RMS roughness measurement in three to five locations of the sample as a function of sampling size

Scan size	RMS roughness, R_q		
(edge length) [μm]	Mean [nm]	Standard deviation [nm]	COV
2	22.1	9.8	0.442
10	52.9	35.0	0.662
50	35.8	9.56	0.267
80	42.1	11.0	0.263

Coefficient of variation (COV) is the standard deviation normalized by the mean.

the $w/c=0.2$ cement paste polished for 8 h. The PDFs, which are more physically intuitive, show the presence of three phases present in the hardened material system, which are referred from left (soft) to right (hard) as the first phase, second phase, and third phase. In this particular sample, the first phase corresponds to a high-density C–S–H phase, the second phase is an ultra-high-density C–S–H phase, and the third phase is the clinker phase [13].

2.4. AFM imaging and roughness analysis

Our primary method of obtaining topographic information about the sample surface is the use of an Atomic Force Microscope (AFM). Topographic images were obtained with a Quesant Q-Scope 250 AFM. The data were acquired using a wavemode, or 'tapping' scan. For each scan, the resolution was 512×512 pixels and the scan rate was 1.0 Hz. Varying scan sizes were used, from 2 μm by 2 μm to 80 μm by 80 μm.

Following the AFM imaging procedure, each file was digitally analyzed in order to extract a roughness value. Before calculation of the roughness, a linear slope correction was performed to account for an alignment difference between the reference plane of AFM imaging and the overall slope of the sample surface. The chosen measurement of roughness was a root-mean-squared average (RMS) of the topography of the surface, R_q, defined by:

$$R_q = \sqrt{\frac{1}{N^2}\sum_{i=1}^{N}\sum_{j=1}^{N} z_{ij}^2} \quad (7)$$

where N is the number of pixels in each scan edge and z_{ij} is the height at position (i, j) from the mean plane. In addition, for images obtained on 80 μm×80 μm and 50 μm×50 μm areas, an 8 μm. Gaussian filter was applied in order to filter out spatial waves having a larger wavelength than 8 μm, which is out of proportion with regard to the characteristic size of our indentations.

To understand the effect of surface roughness on the results of the grid indentation technique on cement pastes, we interrupted the sample preparation procedure at various times to perform nanoindentation and roughness measurements. Specifically, we tested directly after the grinding stage, and after 1 h, 2 h, 4 h, and the full 8 h of polishing.

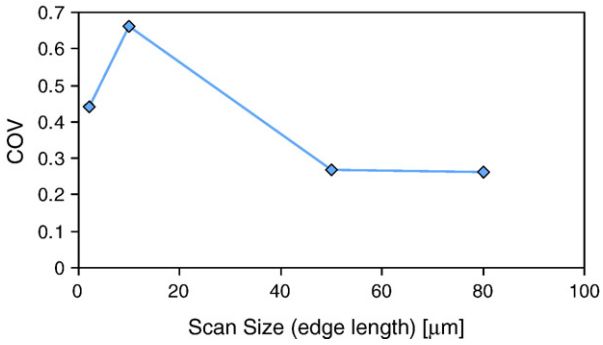

Fig. 6. Coefficient of variation (COV) vs. scan size. The variation is minimized for scan sizes with edge lengths of at least 50 μm.

Following each grid of nanoindentations, 3 topographic images were obtained: one of a 50 μm×50 μm area, one of a 10 μm×10 μm area and one of a 2 μm×2 μm area. In addition, after 4 h of polishing, a number of AFM images were obtained at different locations to assess the variability of the roughness measurement for different scanning sizes. Specifically, three to five topographic images were obtained at different locations using scan sizes of 2 μm×2 μm, 10 μm×10 μm, 50 μm×50 μm, and 80 μm×80 μm.

3. Results

3.1. Variation in roughness values with scan size

Another limitation of the RMS roughness value is that it may exhibit variability from location to location on the sample. The extracted mean and standard deviation of roughness values at different locations for the specimen polished for 4 h are given in Table 1. Interestingly, although there is no clear trend in mean R_q with scan size, there are significant differences between the results from each size.

The tests of roughness at various locations on the same sample suggest that roughness measurements exhibit significant variability. A possible explanation for this variability is that because the cement paste is inherently heterogeneous, the

Table 2
Variability of the RMS roughness measurement for the 50 μm by 50 μm scans with varying resolution

Scan resolution	RMS roughness, R_q		
(pixels×pixels)	Mean [nm]	Standard deviation [nm]	COV
430×430	35.7	9.6	0.268
215×215	35.7	9.6	0.269
143×143	35.6	9.6	0.271
107×107	35.6	9.7	0.272
86×86	35.9	9.5	0.265
71×71	35.3	9.6	0.273
43×43	35.3	9.2	0.262
21×21	34.9	7.9	0.227
10×10	38.5	11.4	0.295

Coefficient of variation (COV) is the standard deviation normalized by the mean.

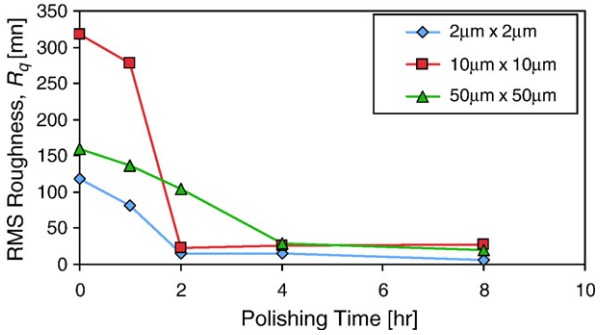

Fig. 7. RMS roughness, R_q, vs. polishing time for three different AFM scan sizes. Roughness is unchanged after 2 to 4 h of polishing.

polished surface is inherently heterogeneous. Overcoming this inherent heterogeneity would require a scan size an order of magnitude larger than the length scale of the largest material phase. In a multiscale material like cement paste [14,2,3], this is not so straightforward. A close examination of the results shown in Fig. 6 sheds some light. The 50 μm × 50 μm and 80 μm × 80 μm scan sizes exhibit the smallest variability because they average over the characteristic length scale of the cement paste and clinker, although there is no advantage to the 80 μm × 80 μm scan size over the 50 μm × 50 μm scan size.

3.2. Variation in roughness values with scan resolution

The effect of scanning resolution on roughness values was investigated by varying the number of rows and columns used to assess roughness at the 50 μm × 50 μm scan size. After filtering, the original 512 × 512 pixel resolution is reduced to 430 × 430 pixels. By removing equally spaced rows and columns, resolution was varied down to only 10 × 10 pixels. Table 2 presents the results of this investigation, and clearly shows that RMS roughness is essentially insensitive to resolution above a minimum of 40 × 40 pixels.

This resolution is well within the capabilities of modern AFM instruments, and higher resolutions produce images which are more easily understood by eye. This low resolution criterion does not justify the use of a much blunter profilometer or Berkovich indenter tip as an adequate substitute for the sharp (less than 20° cone angle, less than 10 nm tip radius) AFM probe, which is capable of measuring topographic features with high spatial frequencies. In this context, a relatively low resolution means that only a random sample of the surface topography is needed to assess the RMS roughness of the surface.

3.3. Roughness and polishing time

The roughness results as a function of polishing time, as detailed in Fig. 7, show that roughness values, in general, decrease sharply over time. Interestingly, after 2 to 4 h of polishing, there is little significant difference in roughness values. Fig. 7 also highlights the observation that the roughness values at different sampling sizes are drastically different. In fact, although roughness values decrease, in general, with time, these data suggest that the rate of decrease is not identical between AFM sampling sizes. This is a first limitation of the RMS roughness value, and suggests that scan size must be reported along with RMS roughness in order to compare values.

3.4. Phase properties: Indentation modulus, hardness and volume fractions

The deconvolution of the nanoindentation tests completes the data set linking roughness and nanoindentation results. Tables 3 and 4 give the indentation modulus and hardness values for each phase, and Table 5 gives the corresponding maximum indentation depths. Fig. 8 illustrates the relationship between decreasing roughness and the convergence of the mean, standard deviation, and volume fraction results to unique, repeatable values. These quantities are graphed vs. the roughness values at 50 × 50 because of the low coefficient of variation in this sampling size (see Table 1). Fig. 8 indicates that, below a roughness of about 100 nm (corresponding to the roughness achieved after 2 h of polishing), the results for the extracted indentation hardness and moduli for the first two peaks are within 5% of the values for the fully (8 h) polished sample. This represents an accuracy similar to the range found in repeatability studies on the same sample. This finding suggests that the longer 8-hour polishing time we suggest is a conservative duration.

Previous research on roughness and nanoindentation has suggested that a rough surface could increase scatter in the data, and cause an overall decrease in measured properties [10,11]. This scatter is evident in the wide variation between the indentation results in the ground, 1 h, and 2 h polishing states. An overall reduction of properties with increased roughness is not apparent, suggesting that a simple correction for surface roughness is impractical, especially for a highly heterogeneous material. On average, with a decrease in surface roughness, there is a decrease in the standard deviation of the indentation modulus and hardness of the peaks.

Table 3
Results of deconvolution of indentation modulus (in GPa) and volume fraction

Polishing time	Peak 1			Peak 2			Peak 3		
	Mean	Standard deviation	f	Mean	Standard deviation	f	Mean	Standard deviation	f
0 h	23.41	16.33	0.23	68.08	23.54	0.61	116.56	24.95	0.16
1 h	17.52	6.43	0.40	36.58	8.30	0.36	72.93	25.62	0.25
2 h	43.83	6.77	0.60	67.88	6.46	0.10	114.27	32.070	0.30
4 h	44.28	7.42	0.59	60.53	8.84	0.12	120.97	23.29	0.29
8 h	43.00	7.07	0.59	63.70	12.80	0.17	126.30	20.16	0.2

Table 4
Results of deconvolution of hardness (in GPa) and volume fraction

Polishing time	Peak 1			Peak 2			Peak 3		
	Mean	Standard deviation	f	Mean	Standard deviation	f	Mean	Standard deviation	f
0 h	0.51	0.36	0.23	2.99	1.42	0.61	6.81	1.80	0.16
1 h	0.46	0.22	0.40	1.15	0.43	0.36	2.90	1.32	0.25
2 h	1.74	0.47	0.60	3.33	0.49	0.10	8.04	2.48	0.30
4 h	1.88	0.42	0.59	3.34	0.46	0.12	8.64	2.21	0.29
8 h	1.59	0.39	0.59	2.96	0.98	0.17	8.94	1.65	0.24

The most dramatic differences in the results came from variations in the volume fractions of the three phases with respect to surface roughness. Fig. 9 illustrates that, in terms of volume fractions, the ground sample shows little relation to the fully polished sample. Yet, the volume fraction results after just 2 h of polishing resemble the fully polished sample results. This result indicates that a relatively short polishing time suffices to achieve reasonably accurate volume fraction data.

At a scan size of 50, it becomes clear that at roughness R_q lower than 50 nm, the results have stabilized. This roughness corresponds to 4 h of polishing. This convergence of material property values occurs before the sample appears smooth by visual observation. As a result, satisfying the visual check for a mirror-like finish that reflects overhead light is a conservative rule-of-thumb for successful indentations of the size considered here.

4. Discussion: RMS roughness criteria for nanoindentation

The main control variables in this study are the nine material phase properties obtained from nanoindentation on the fully polished sample. Specifically, these are the three peak values for indentation modulus, the three peak values for hardness, and the three surface fractions. These nine values are obtained from statistical distributions derived from 300 indentations on each sample surface. The overall goal of any roughness criterion is to achieve nanoindentation results that match the true properties of the material.

The RMS roughness value is best used as a qualitative or comparative measure for nanoindentation because of two main problems with this measure of topological variation. First, there is significant spatial variation of the samples at the tested scales. Second, the measured roughness depends greatly on the chosen scan size. As indicated, the variability and magnitude of RMS roughness R_q is different at different scan sizes. In addition, the rate of decrease of roughness appears to vary depending on the scan area.

It is clear that a criterion for roughness is complicated not only by the choice of scan size, but also by the choice of indentation depth. These choices are in turn complicated by the multiscale nature of cement paste [14]. Our results indicate that any criterion requiring that an indentation depth, h, be greater than some factor of RMS roughness, R_q, is insufficient for quantifying an independence of roughness from nanoindentation results on heterogeneous materials. Such a quantification should also depend on the sampling size of the AFM imaging

Table 5
Results of deconvolution of maximum indentation depth (in nm) and RMS roughness (in nm)

Polishing time	Peak 1		Peak 2		Peak 3		R_q
	Mean	Standard deviation	Mean	Standard deviation	Mean	Standard deviation	(50 scan size)
0 h	471	106	178	39	128	10	159
1 h	495	115	306	66	190	51	136
2 h	235	28	188	19	117	17	104
4 h	220	26	170	25	108	8	29
8 h	241	28	187	26	110	7	20

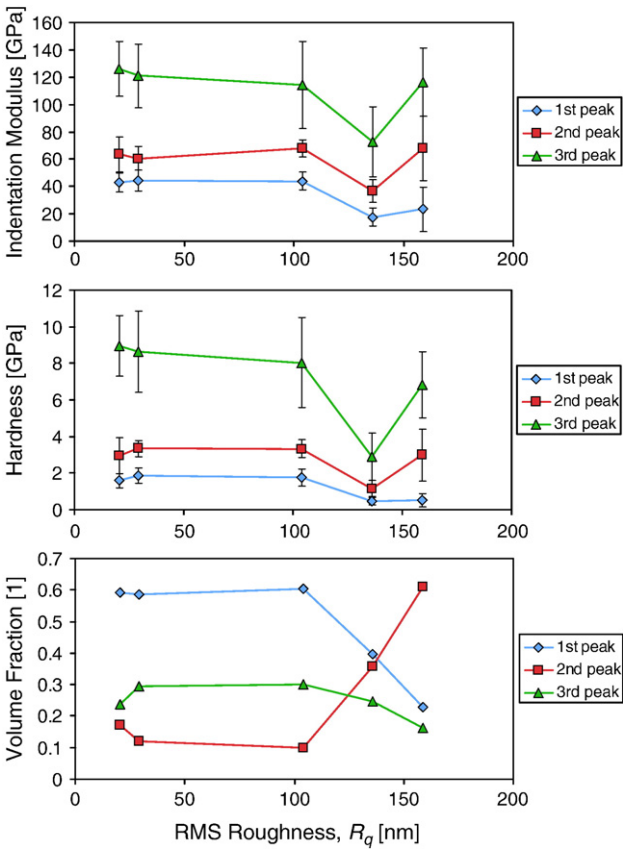

Fig. 8. Nanoindentation deconvolution results vs. RMS Roughness, R_q. Top: Average indentation modulus, M, of each phase. Middle: Average hardness, H, for each phase. Bottom: Volume fraction of each phase. The error bars in indentation modulus and hardness represent plus and minus one standard deviation. The mean properties and volume fractions converge to within about 5% of the final values when the RMS roughness is less than 100 nm.

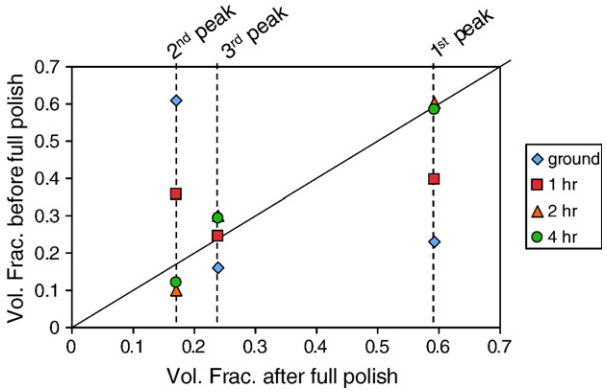

Fig. 9. Extracted volume fractions at different stages of the polishing process vs. extracted volume fractions after a full, 8 h polishing procedure. Volume fractions after 2 h of polishing are similar to those after the full 8 h.

and on which material phases are used to determine the average indentation depth. The discussion of variability of R_q with scan size indicates that an AFM scan with an edge length of 50 minimizes variation between scans. The indentation depths, h, for the fully polished specimen are approximately 240 nm for the first phase, 190 nm for the second phase, and 110 nm for the third phase. This means that the scanning edge length, l, should be at least $200h$ for an average h from the first phase, at least $250h$ for an average h from the second phase, and at least $450h$ for an average h from the third phase. This assures that the roughness measurement assesses a surface size on an order greater than the length scale of the largest material heterogeneity. The discussion of convergence of material properties indicates that convergence occurs once R_q is less than 50 nm. Thus, the first phase converges after $h>5R_q$, the second phase begins to converge when $h>4R_q$ and, the third phase, with its shallow indentation depth, converges after $h>2R_q$.

We select the indentation depth of the dominating, first phase as the basis for comparison. As a result, we propose standardizing the scanning edge length, l, to $200h$ where h is the average indentation depth of the dominating first phase. With the sampling size and indentation depth parameters standardized, material properties appear to converge to a unique set of values when $h>5R_q$.

5. Conclusion

This study suggests that the RMS roughness, as currently measured, is only an approximate indicator of a surface's suitability for nanoindentation, but it is a simple measurement that can be easily repeated in many different labs. The measurement has been used to develop an optimized surface preparation procedure for nanoindentation of cement pastes, consisting of two repeatable steps. First, the sample is made flat and parallel to a mount by grinding on sandpaper. This is followed by a slow polish with 1 μm diamond paste on a hard, perforated pad. After a relatively short polishing duration, 2–4 h, the extracted material properties are similar to the results of any longer polishing durations. The full 8 h polishing time, which gives a reflective surface, is a conservative duration.

An accurate and repeatable topological characterization measurement is still an enigma. The RMS roughness measurement shows a non-negligible variability, and is highly dependent on the scanning size. Possible alternatives to quantification of roughness include performing a statistical analysis of curvature or surface slopes, and future work in this area is encouraged.

Given that such an alternative is still in the future, a criteria for RMS roughness must include the scanning size on which the measurement is based. For cement paste and other multiscale materials, this scanning size must be balanced with the other scale separability requirements for grid nanoindentation. The results presented here indicate that material properties obtained from nanoindentation converge to a unique set of values when the average indentation depth of the first peak, h, is greater than 5 times the RMS roughness, R_q where the roughness is measured over a scanning size 200 times h.

Acknowledgement

The authors gratefully acknowledge the Lafarge Group for providing the financial support for this research with Jean-François Batoz as Technical Advisor and Dr. Paul Acker as Scientific Advisor. The tested cement paste was prepared by Dr. Philippe Fonollosa (Lafarge). The authors also thank Alan Schwartzman, director of the NanoMechanical Laboratory at MIT, for the assistance with AFM testing. Further support was provided by Ecole Nationale des Ponts et Chaussees (France), enabling M. Vandamme's doctoral studies at MIT.

References

[1] G. Constantinides, F.J. Ulm, K. Van Vliet, On the use of nanoindentation for cementitious materials, Mat. Struct. 36 (257) (2003) 191–196 (2003).
[2] G. Constantinides, F.J. Ulm, The effect of two types of C–S–H on the elasticity of cement-based materials: results from nanoindentation and micromechanical modeling, Cem. Concr. Res. 34 (1) (2004) 67–80.
[3] G. Constantinides, F.J. Ulm, The nanogranular nature of C–S–H, J. Mech. Phys. Solids 55 (1) (2007) 64–90.
[4] M.J. DeJong, F.J. Ulm, The nanogranular behavior of C–S–H at elevated temperatures (up to 700C), Cem. Concr. Res. 37 (1) (2007) 1–12.
[5] F.J. Ulm, M. Vandamme, C. Bobko, J.A. Ortega, K. Tai, C. Ortiz, Statistical indentation techniques for hydrated nanocomposites: concrete, bone, and shale, J. Am. Ceram. Soc. 90 (9) (2007) 2677–2692.
[6] G. Constantinides, K.S. Ravi Chandran, F.J. Ulm, K.J. Van Vliet, Grid indentation analysis of composite microstructure and mechanics: principles and validation, Mater. Sci. Eng., A 430 (1–2) (2006) 189–202.
[7] W.C. Oliver, G.M. Pharr, An improved technique for determining hardness and elastic modulus using load and displacement sensing indentation experiments, J. Mater. Res. 7 (6) (1992) 1564–1583.
[8] F.M. Borodich, L.M. Keer, C.S. Korach, Analytical study of fundamental nanoindentation test relations for indenters of non-ideal shapes, Nanotechnology 14 (2003) 803–808.
[9] Y.T. Cheng, C.M. Cheng, Scaling, dimensional analysis and indentation measurements, Mater. Sci. Eng., R 44 (2004) 91–149.
[10] M.S. Bobji, S.K. Biswas, Deconvolution of hardness from data obtained from nanoindentation of rough surfaces, J. Mater. Res. 14 (6) (1999) 2259–2268.
[11] J.U. Kim, J.J. Lee, Y.H. Lee, J. Jang, D. Kown, Surface roughness effect in instrumented indentation: a simple contact depth model and its verification, J. Mater. Res. 21 (12) (2006) 2975–2978.
[12] E. Donnely, S.P. Baker, A.L. Boskey, M.C.H. van der Meulen, Effects of surface roughness and maximum load on the mechanical properties of

cancellous bone measured by nanoindentation, J. Biomed. Mater. Res., A 77 (2) (2006) 426–435.
[13] F.J. Ulm, M. Vandamme, C. Bobko, J.A. Ortega, K. Tai, C. Ortiz, Statistical indentation techniques for hydrated nanocomposites: concrete, bone, and shale, J. Am. Ceram. Soc, 90 (9) (2007) 2677–2692.
[14] F.J. Ulm, G. Constantinides, F.H. Heukamp, Is concrete a poromechanics material? — A multiscale investigation of poroelastic properties, Mat. Struct. 37 (265) (2004) 43–58.
[15] ISO-14577-1, Metallic Materials — Instrumented Indentation Test for Hardness and Materials Parameters — Part 1: Test Method, Geneva, Switzerland, 2002.
[16] P. Grau, C.h. Ullner, H.H. Behncke, Uncertainty of depth sensing hardness, Materialprüfung 39 (9) (1997) 362–367.
[17] L.D. Mitchell, M. Prica, J.D. Birchall, Aspects of Portland cement hydration studied using Atomic Force Microscopy, J. Mater. Sci. 31 (1996) 4207–4212.
[18] T. Yang, B. Keller, E. Magyari, AFM investigation of cement paste in humid air at different relative humidities, J. Phys., D, Appl. Phys. 35 (2002) L25–L28.
[19] V.G. Papadakis, E.J. Pedersen, H. Lindgreen, An AFM–SEM investigation of the effect of silica fume and fly ash on cement paste microstructure, J. Mater. Sci. 34 (1999) 683–690.
[20] C. Plassard, E. Lesniewska, I. Pochard, A. Nonat, Nanoscale experimental investigation of particle interactions at the origin of the cohesion of cement, Langmuir 21 (2005) 7263–7270.
[21] B. Jönsson, A. Nonat, C. Labbez, B. Cabane, H. Wennerström, Controlling the cohesion of cement paste. Langmuir 21 (2005) 9211–9221.
[22] C. Plassard, E. Lesniewska, I. Pochard, A. Nonat, Investigation of the surface structure and elastic properties of calcium silicate hydrates at the nanoscale, Ultramicroscopy 100 (2004) 331–338.